# An integral representation of the Green's function for a linear array of acoustic point sources

Harun Kurkcu [a,*] and Nilima Nigam [a] and Fernando Reitich [b]

[a] *Department of Mathematics, Simon Fraser University, 8888 University Drive, Burnaby, BC, V5A 1S6, Canada*

[b] *School of Mathematics, University of Minnesota, Minneapolis, MN 55455, United States*

**Abstract**

We present a new algorithm for the evaluation of the periodized Green's function for a linear array of acoustic point sources such as those arising in the analysis of line array loudspeakers. A variety of classical algorithms (based on spatial and spectral representations, Ewald transformation, etc.) have been implemented in the past to evaluate these acoustic fields. However as we show, these methods become unstable and/or impractically expensive as the frequency of use of the sources increases. Here we introduce a new numerical scheme that overcomes some of these limitations allowing for simulations at unprecedentally large frequencies. The method is based on a new integral representation derived from the classic spatial form, and on suitable further manipulations of the relevant integrands to render the integrals amenable to efficient and accurate approximations through standard quadrature formulas. We include a variety of numerical results that demonstrate that our algorithm compares favorably with several classical method both for points close to the line where the poles are located and at high-frequencies while remaining competitive with them in every other instance.

*Key words:* Green's function periodic domain, rough-surface, high-frequency, free-space, Helmholtz equation.

* Corresponding author.

*Email addresses:* hka50@sfu.ca (Harun Kurkcu), nigam@math.sfu.ca (Nilima Nigam), reitich@math.umn.edu (Fernando Reitich).

## 1 Introduction

The evaluation of the potential due to an infinite number of acoustic point sources arranged periodically along a line in three space dimensions presents numerical challenges. Knowledge of this potential is useful, for example, in the design of line array loudspeakers. These are collections of speakers arranged in a vertical or horizontal configuration; patterns of constructive and destructive interference lead to more directionality and sound intensity compared to a single speaker. The effects of increased directionality was documented by [1]. Another interesting feature of these speakers is that in certain limits, the intensity of acoustic power varies inversely with the distance, rather than inversely with the square of the distance as one might expect with a radiating point source. Since the 1960's, such line array speakers have become popular especially in large venues. Challenges arise with faithful sound reproduction in the near field as well as in the high frequency domain, and the ability to rapidly and accurately compute the potential due to such an arrangement of sources is key in the optimal design of such speakers. In this paper we introduce a novel method for the evaluation of this potential (the Green's function). The method is applicable even in the regimes where existing methods are not competitive.

The general area of computing periodized Green's functions has attracted significant attention from engineers and mathematicians over the last 40 years and has resulted in some novel methods, including the work in [2–4] for two-dimensional problems with one-dimensional periodicity (i.e., a planar array of line sources) and [5,6] for three-dimensional problems with two-dimensional periodicity (i.e., a planar array of point sources). Indeed, while the present paper describes an intermediate problem of one-dimensional periodicity in three dimensions [7], part of the motivation is to use this method as a building block for the full three-dimensional problem with two-dimensional periodicity.

The classical algorithms based on using spatial or spectral representations, or the Ewald's transform [7], result in series with slowly decaying terms. We shall show that these algorithms develop problems especially in the extremely near-field, as well as at high-frequencies.

The method we introduce can effectively provide solutions at very high-frequencies or in the very near field, while remaining competitive with the optimal choices of currently available schemes throughout their domain of applicability. Briefly, the method begins with a new integral representation similar to one developed in [8] for the case of a planar array of line sources. The method is based on the spatial representation of the Green's function, $G$, from which an integral representation is derived. The integrand in the latter is an exponentially decaying function $f(x, y, z; u)$ for $u \geq 0$ where $(x, y, z)$ denote the spatial variables and the sources are placed along the $z-$axis. At low-frequencies and/or for small

values of the distance $\rho = \sqrt{x^2 + y^2}$ the function $f$ and its derivatives remain bounded and a standard quadrature can provide an efficient means to evaluate the integral. As the frequency increases, the integrand $f$ displays progressively larger and more rapid oscillations which cancel out to produce a significantly smaller integrated value. In this case classical quadratures tend to be unstable and inadequate. To overcome these difficulties our scheme is based on polynomial expansions of quotients of $f$ and suitably chosen functions to allow for explicit evaluations, and on judicious integration by parts in order to improve stability and reduce the computational cost.

The rest of the paper is organized as follows. First, and for the sake of completeness, in §2 we briefly review the most popular methods that have been devised to compute $G$, including those based on spatial and spectral representations, and on the Ewald transform. We discuss the problems that arise with each of these, either as the observation point approaches the array or as the frequency increases. In section §3 we derive a new integral representation and §4 is devoted to the presentation of our new high-frequency algorithm. Finally in §5 we present numerical results that confirm that this method significantly outperforms classical procedures. As we show, the method enables accurate simulations even in the regimes where other methods fail.

## 2 Problem statement and review of existing algorithms

In this paper, we are concerned with the problem of evaluating the scalar potential due to point sources arrayed along a line with equal spacing. These sources are assumed to be operating with equal amplitude and with phases that are allowed to vary linearly with the source location. In [1], the characteristic features of such line arrays are described. For example, the directional behavior of such an array is observed only within a range of frequencies. In order to maintain directionality at high frequencies, it is known that the spacing between the sources must be reduced.

We will be working in the frequency domain, and thus a time dependence of $e^{-i\omega t}$ has been factored out. The point sources are assumed to be located at positions $nd\hat{k}$ for $n \in \mathbb{Z}$, $d > 0$. There is thus a natural periodicity with period $d$ in the $z$ direction. We assume further that the line array is embedded in a medium with background wave number $k$, and we are interested in the outgoing solution of the Helmholtz equation.

The problem can be rephrased in terms of a Green's function $G(x, y, z)$: Find

the solution of

$$\Delta G(x,y,z) + k^2 G(x,y,z) = -\sum_{n=-\infty}^{\infty} \exp(i\alpha n d)\delta(x)\delta(y)\delta(z-nd),$$

where the $nth$ point source is located at $R_n = nd\hat{k}$, $\alpha = k\sin(\theta)$ for a fixed incidence angle $\theta$, and the potential is being evaluated at point $(x,y,z)$. Given the axial symmetry in the problem, it is appropriate to use cylindrical coordinates. The observation point $(x,y,z)$ is therefore $(x,y,z) = \rho\hat{\rho} + z\hat{k}$. We also need to specify a radiation condition and to derive this relation we note the periodicity of the structure implies that the fields can be represented as Fourier-like series. Indeed letting,

$$\alpha_n = \alpha + \frac{2\pi n}{d} \text{ and } \beta_n = \sqrt{k^2 - \alpha_n^2}$$

we have

$$G(\rho,z) = \sum_{n=-\infty}^{\infty} A_n e^{i\alpha_n z} H_0^{(1)}(\beta_n \rho) + \sum_{n=-\infty}^{\infty} B_n e^{i\alpha_n z} H_0^{(2)}(\beta_n \rho),$$

where

$$H_0^{(1,2)}(z) = J_0(z) \pm iY_0(z)$$

and $J_0(z)$, $Y_0(z)$ are the zeroth order Bessel functions of the first and second kind respectively. In terms of Fourier coefficients the radiation condition (outgoing field) can be stated as

$$B_n = 0 \text{ for all } n.$$

Note that radiation may propagate axially along the array (as a Floquet wave).

We shall now describe some popular representations of $G(\rho,z)$ which are used in some existing numerical strategies. We discuss the difficulties which arise in the high frequency (large $k$) and nearly-axial (small $\rho$) regimes. In each case, these difficulties lead to an increase in computational cost and/or the deterioration of the stability properties of these methods.

**1. Spatial representation:** The simplest method for evaluating $G(\rho,z)$ follows from the explicit knowledge of the free-space Green function $G_s$with a single point source located at the origin: $G_s(x,y,z) = G_s(\rho,z) = \frac{e^{ik\sqrt{\rho^2+z^2}}}{4\pi\sqrt{\rho^2+z^2}}$. For an array of such point sources, we can simply add these contributions. For fixed $\alpha$ and wave number $k$,

$$G(\rho,z) = \frac{1}{4\pi}\sum_{n=-\infty}^{\infty} e^{i\alpha n d}\frac{e^{ikr_n}}{r_n} \tag{1}$$

where

$$r_n = \sqrt{\rho^2 + (z - nd)^2}.$$

The terms of this series only decay as $\frac{1}{n}$, and the series does not converge absolutely. Therefore, summation of this series is an inefficient technique at best; the problems are independent of frequency. More precisely

$$\left| G(\rho, z) - \frac{1}{4\pi} \sum_{n=-N}^{N} e^{i\alpha nd} \frac{e^{ikr_n}}{r_n} \right| \sim \left| \frac{1}{2\pi} \frac{e^{i(k+\alpha d)(N+1)}}{N+1} \right| = \frac{1}{2\pi(N+1)} \qquad (2)$$

and

$$G(\rho, z) \sim \frac{1}{4\pi} \frac{e^{ikr_0}}{r_0}.$$

**2. Spectral representation:** Another approach for computing $G$ relies on its Fourier series representation [7]. Since $G$ is a (quasi) periodic function, one can easily use Poisson's summation formula to obtain a "spectral representation":

$$\sum_{n=-\infty}^{\infty} f(nd) = \frac{1}{d} \sum_{q=-\infty}^{\infty} \tilde{f}(\frac{2\pi}{d} q),$$

where

$$f(nd) = e^{i\alpha nd} \frac{e^{ikr_n}}{4\pi r_n}, \qquad r_n = \sqrt{\rho^2 + (z - nd)^2},$$

and

$$\tilde{f}(\frac{2\pi}{d} q) = \frac{1}{4id} \int_{-\infty}^{\infty} e^{i\frac{2\pi}{d} qu} f(u) du.$$

Specifically, this spectral representation becomes

$$G(\rho, z) = \frac{1}{4id} \sum_{n=-\infty}^{\infty} e^{i\alpha_n z} H_0^{(1)}(\beta_n \rho), \qquad (3)$$

where $H_0^{(1)}$ is the zeroth order Hankel function of the first kind. The $n$-th Floquet wave number along the axial ($z$) direction is

$$\alpha_n = \alpha + \frac{2\pi}{d} n,$$

and the $n$-th transverse Floquet wave number is

$$\beta_n = \sqrt{k^2 - \alpha_n^2} = \sqrt{k^2 - (\alpha + \frac{2\pi}{d} n)^2}.$$

In contrast with the representation in (1) the series in (3) converges exponentially for $\rho > 0$. If $\alpha$ is real and the medium is lossless ($k$ is real), then for

$\alpha_n^2 < k^2$ the $\beta_n$ describe radially propagating waves, while for $\alpha_n^2 > k^2$ the $\beta_n$ index Floquet waves attenuating in the $\rho$ direction. The critical index is

$$N = \frac{|k|d - \alpha d}{2\pi};$$

for $|n| > N$ the terms in the series (3) decay exponentially, corresponding to the attenuating Floquet modes. This is easily seen from the asymptotic behavior of the Hankel function,

$$H_0^{(1)}(a) \sim \sqrt{\frac{2}{\pi a}} e^{i(a-\frac{\pi}{4})} \quad \text{for } 1 \ll |a| \text{ [9, Equation 9.2.3].}$$

Clearly if $\beta_n$ is complex-valued, which happens for $|n| > N$, $H_0^{(1)}(\beta_n \rho)$ is an exponentially small term *provided* $\rho > 0$. The method does not converge if $\rho = 0$.

It is worth examining the computational cost of this method. We would need to retain, at a minimum, enough terms $n$ in the series such that $|\beta_n|\rho > 1$. For example, $n > N$ must be chosen large enough such that

$$|\beta_n|\rho = \left|\sqrt{k^2 - (\alpha + \frac{2\pi}{d}n)^2}\right| \rho > 1 \text{ or, equivalently } n > 2N + \frac{2}{\rho\frac{2\pi}{d}\left(k\rho + \sqrt{k\rho^2+1}\right)}.$$

Clearly if $k$ is large, or $\frac{\rho}{d}$ is small, $n$ must be chosen to be large enough to provide accurate results.

**3. <u>Ewald transformation:</u>** The Ewald summation technique for this problem due to Capalino et. al. [7] is based on the integral representation

$$\frac{e^{ikr}}{4\pi r} = \frac{1}{2\pi^{3/2}} \int_0^\infty e^{-r^2 s^2 + \frac{k^2}{4s^2}} ds,$$

to accelerate the convergence of the spatial representation series in (1). To review this approach, let us begin with fixing $E > 0$, and defining

$$G_{\text{spectral}}(\rho, z) = \frac{1}{2\pi\sqrt{\pi}} \sum_{n=-\infty}^{\infty} e^{i\alpha n d} \int_0^E e^{-r_n^2 s^2 + \frac{k^2}{4s^2}} ds,$$

and

$$G_{\text{spatial}}(\rho, z) = \frac{1}{2\pi\sqrt{\pi}} \sum_{n=-\infty}^{\infty} e^{i\alpha n d} \int_E^\infty e^{-r_n^2 s^2 + \frac{k^2}{4s^2}} ds,$$

where $r_n = \sqrt{\rho^2 + (z - nd)^2}$ so that, from (1),

$$G(\rho, z) = G_{\text{spectral}}(\rho, z) + G_{\text{spatial}}(\rho, z). \tag{4}$$

Next we note that the series $G_{\text{spectral}}(\rho, z)$ rewritten as

$$G_{\text{spatial}}(\rho, z) = \frac{1}{8\pi} \sum_{n=-\infty}^{\infty} \frac{e^{i\alpha nd}}{r_n} \left[ e^{-ikr_n} \text{erfc}(Er_n - i\frac{k}{2E}) + e^{ikr_n} \text{erfc}(Er_n + i\frac{k}{2E}) \right], \tag{5}$$

where $\text{erfc}(a)$ is the complementary error function. The other series $G_{\text{spectral}}$, in turn, can be written as

$$G_{\text{spectral}}(\rho, z) = \frac{1}{4\pi d} \sum_{n=-\infty}^{\infty} e^{i\alpha_n d} \sum_{m=0}^{\infty} \frac{(-1)^m}{m!} (\rho E)^{2m} E_{m+1}(-\frac{\beta_n^2}{4E^2}), \tag{6}$$

where the $m$th order exponential integral $E_m(x)$ is defined by

$$E_m(x) = \int_1^{\infty} u^{-m} e^{-xu} du.$$

Now, the combined exponential decay of the series (5) and (6) make this into a efficient method for moderate values of $k$. In this case, it can be shown that the optimal choice of $E$ is

$$E = \frac{\sqrt{\pi}}{d}, \tag{7}$$

in which case both series converge at the same asymptotic rate [7]. However, as also shown in [7], this choice of the parameter $E$ leads to unstable evaluations for larger frequencies and must be modified to ensure the boundedness of the terms in the series. More precisely, we have

$$\text{erfc}(a) \sim e^{-a^2}/\sqrt{\pi a} \text{ and } E_1(a) \sim e^{-a}/a \text{ for } |a| \gg 1,$$

so that, for large $k$,

$$G_{\text{spatial}}(\rho, z) \sim \sum_n e^{\frac{k^2}{4E^2} - E^2(\rho^2 + (z-nd)^2)},$$

and

$$G_{\text{spectral}}(\rho, z) \sim \sum_n \frac{4E^2}{k^2 - (\alpha + np)^2} e^{\frac{k^2 - (\alpha+np)^2}{4E^2}}.$$

Thus, for large $k$, a choice of $E$ that is independent of frequency (such as that in (7) leads to large values of the terms in the series (5) and (6) and to inaccurate values of the $G(\rho, z)$ as a result of cancellations. To avoid this difficulty, one may choose

$$E = \max \left\{ E_{\text{spectral}} = \frac{C_1\sqrt{k}}{\sqrt{2\sqrt{\rho^2 + z^2}}},\ E_{\text{spatial}} = \frac{C_2\sqrt{k^2 - \alpha^2}}{2} \right\} \tag{8}$$

for some constants $C_{1,2}$ which are related to the maximum allowable value of the terms in (5) and (6).

As can be easily verified this choice will allow evaluations of $G_{\text{spatial}}(\rho, z)$ with a computational cost independent of frequency and will put the computational burden on the calculation of $G_{\text{spectral}}(\rho, z)$. In detail, we can approximate

$$G_{\text{spectral}} \approx \frac{1}{4\pi d} \sum_{n=-N}^{N} e^{i\alpha_n d} \sum_{m=0}^{\infty} \frac{(-1)^m}{m!} (\rho E)^{2m} E_{m+1}(-\frac{\beta_n^2}{4E^2}) \tag{9}$$

to within an accuracy of $\epsilon$ provided

$$N \geq \log(\epsilon) k$$

And this, in turn, leads to a computational cost that is similar to that of evaluation of standard spectral series (3).

Moreover, once $E$ chosen as in (8), its stability properties deteriorate significantly for large $k$ due to the correspondingly large values of

$$\frac{(\rho E)^{2m}}{m!} \sim \max \left\{ \frac{\left(k\rho^2/\sqrt{\rho^2+z^2}\right)^m}{m!}, \frac{(k\rho)^{2m}}{m!} \right\} \tag{10}$$

in the inner sum (9), (see also [7, §4.2]) resulting an unavoidable loss of accuracy in its evaluation.

## 3 A new integral representation of the Green's function

In this section we will derive an alternative representation for the Green's function for a line array. This representation will form the backbone of our computational method. As in [8], the starting point for this derivation is the spatial form (1), and the simple observation that

$$\sum_{n=1}^{\infty} e^{-ian} e^{nv} = \frac{e^{-ia}}{e^v - e^{-ia}}.$$

If $L(f)$ is the Laplace transform of a function $f$, then we can use the identity above to get

$$\sum_{n=1}^{\infty} e^{-ian} F(n) = e^{-ia} \int_0^{\infty} \frac{f(v)}{e^v - e^{-ia}} dv.$$

For our purposes, we use the identity [10, Equation 4.146.1]

$$L^{-1}\{e^{\beta m} \frac{e^{-\beta\sqrt{m^2+\gamma^2}}}{\sqrt{m^2+\gamma^2}}\} = J_0(\gamma\sqrt{v^2+2\beta v})$$

to see that for $n > 0$, the sum in (1) becomes

$$\sum_{n=1}^{\infty} e^{i\alpha nd}\frac{e^{ikr_n}}{r_n} = \int_0^{\infty} \frac{e^{ikd}}{e^v - e^{ikd}} \left(\frac{1}{d}e^{-ikz+\frac{z}{d}v} J_0\Big(\rho\sqrt{(\frac{v}{d})^2 - 2ik\frac{v}{d}}\Big)\right) dv.$$

We can use a similar argument for the remaining terms of the sum in (1):

$$\begin{aligned}\sum_{n=-\infty}^{-1} e^{i\alpha nd}\frac{e^{ikr_n}}{r_n} &= \sum_{n=1}^{\infty} e^{-i\alpha nd}\frac{e^{ik\sqrt{(z+nd)^2+\rho^2}}}{\sqrt{(z+nd)^2+\rho^2}} \\ &= \int_0^{\infty} \frac{e^{i(k-\alpha)d}}{e^v - e^{i(k-\alpha)d}} \left(\frac{1}{d}e^{ikz-\frac{z}{d}v} J_0\Big(\rho\sqrt{(\frac{v}{d})^2 - 2ik\frac{v}{d}}\Big)\right) dv\end{aligned}$$

Putting these expressions together, the Green's function $G(\rho, z)$ can be written as

$$\begin{aligned}G(\rho,z) &= \frac{1}{4\pi}\frac{e^{ikr_0}}{r_0} \\ &+ \frac{e^{ikz}}{4\pi d}\int_0^{\infty} \frac{e^{i(k-\alpha)d}}{e^v - e^{i(k-\alpha)d}} e^{-\frac{z}{d}v} J_0\Big(\rho\sqrt{(\frac{v}{d})^2 - 2ik\frac{v}{d}}\Big)dv \\ &+ \frac{e^{-ikz}}{4\pi d}\int_0^{\infty} \frac{e^{i(k+\alpha)d}}{e^v - e^{i(k+\alpha)d}} e^{\frac{z}{d}v} J_0\Big(\rho\sqrt{(\frac{v}{d})^2 - 2ik\frac{v}{d}}\Big)dv.\end{aligned}$$

Next, a change of variables $v = kd\zeta^2$ is applied to put this in a more convenient form

$$G(\rho,z) = \frac{1}{4\pi}\frac{e^{ikr_0}}{r_0} + \frac{k}{2\pi}\left[\int_0^{\infty} f^{(1)}(\zeta)d\zeta + \int_0^{\infty} f^{(2)}(\zeta)d\zeta\right] \tag{11}$$

with

$$f^{(a)}(\zeta) = \zeta e^{i(2a-3)kz}\frac{e^{i(k-(2a-3)\alpha)d}e^{-(2a-3)kz\zeta^2}}{e^{kd\zeta^2} - e^{i(k-(2a-3)\alpha)d}} J_0\Big(k\rho\zeta\sqrt{\zeta^2 - 2i}\Big), \tag{12}$$

for $a = 1, 2$ which provides the desired representation.

## 4 A new algorithm

In this section we provide a derivation of a new procedure based on the new integral representation described in the previous section. More precisely, it relies on further manipulation of the integrals in (11) in a manner so as to reduce the integration problem to one where the application of classical quadrature formulas becomes simultaneously stable and efficient.

In what follows, and for the sake of the presentation, we shall assume $\alpha = 0$, and focus on the plane $z = 0$. The arguments for other values of $\alpha$ and $z$ follow

largely along the same lines. In this case, we note that $G(\rho, 0)$ in (11) can be rewritten as

$$G(\rho, 0) = \frac{1}{4\pi}\frac{e^{ik\rho}}{\rho} + \frac{k}{\pi} I_\infty \tag{13}$$

where

$$I_\infty = \int_0^\infty f(\zeta) d\zeta \text{ and } f(\zeta) = \zeta \frac{J_0\Big(k\rho\zeta\sqrt{\zeta^2 - 2i}\Big)}{e^{kd(\zeta^2 - i)} - 1}. \tag{14}$$

**Lemma 4.1** *Given $\epsilon > 0$, there exists a $C \in \mathbb{R}$ such that*

$$|\int_0^\infty f(\zeta) d\zeta - \int_0^C f(\zeta) d\zeta| < \epsilon \frac{\sqrt{\pi}}{\sqrt{4kd}} \tag{15}$$

*where $C$ satisfies*

$$\frac{e^{k\rho C}}{e^{kdC^2}} = \epsilon \text{ or, equivalently, } C = \frac{\rho + \sqrt{\rho^2 - \frac{4d\log(\epsilon)}{k}}}{2d}. \tag{16}$$

To see (4.1), we will use

$$|J_0(a)| \le e^{|\Im(a)|} \text{ for all } a \text{ [9, Equation 9.1.62] },$$
$$|\Im(\zeta\sqrt{\zeta^2 - 2i})| = \zeta\sqrt{\frac{2}{\zeta^2 + \sqrt{\zeta^2 + 4}}} \le \min\{\zeta, 1\} \text{ for all } \zeta \ge 0,$$

and

$$\zeta e^{k\rho \min\{\zeta, 1\}} \le e^{k\rho\zeta} \text{ for all } \zeta \ge 0.$$

From these it follows

$$|\zeta \frac{J_0\Big(k\rho\zeta\sqrt{\zeta^2 - 2i}\Big)}{e^{kd(\zeta^2 - i)} - 1}| \le |\frac{\zeta e^{k\rho\zeta\sqrt{2/(\zeta^2 + \sqrt{\zeta^2 + 4})}}}{e^{kd(\zeta^2 - i)} - 1}| \le |\frac{\zeta e^{k\rho\min\{\zeta,1\}}}{e^{kd(\zeta^2 - i)} - 1}| \le |\frac{e^{k\rho\zeta}}{e^{kd(\zeta^2 - i)} - 1}|.$$

Finally,

$$|\int_C^\infty f(\zeta)\, d\zeta| \le \int_C^\infty |f(\zeta)|\, d\zeta \le 2\int_C^\infty \exp(k\rho\zeta - kd\zeta^2)\, d\zeta \le \epsilon\frac{\sqrt{\pi}}{\sqrt{4kd}}$$

since

$$|\frac{1}{e^{kd(\zeta^2 - i)} - 1}| \le |\frac{2}{e^{kd(\zeta^2 - i)}}| \text{ for } u \ge C \text{ if } \epsilon \le 1,$$

and

$$\int_C^\infty \frac{e^{k\rho\zeta}}{e^{kd\zeta^2}}\, d\zeta = \frac{e^{k\rho C}}{e^{kdC^2}} \int_0^\infty \frac{e^{k\rho v - 2kdCv}}{e^{kdv^2}}\, dv \le \epsilon\frac{\sqrt{\pi}}{\sqrt{4kd}}$$

provided $C$ is chosen as in (16). Thus, it suffices to design an efficient way to evaluate

$$I = \int_0^C f(\zeta) d\zeta. \tag{17}$$

To do this we first we note that

$$|\int_0^\infty f(\zeta)d\zeta| \sim \frac{1}{kd} \text{ as } k \to \infty$$

and

$$\max|f(\zeta)| \sim \frac{e^{k\rho^2/4d}}{\sqrt{\pi kd}} \text{ and } \max|f'(\zeta)| \sim e^{\frac{k\rho^2}{4d}}. \tag{18}$$

To see (18) we look at the behavior of the integrand given in (13). For $\zeta \sim 0$ we have that

$$k\rho\zeta\sqrt{\zeta^2 - i} \sim k\rho\zeta(1-i),$$

and for fixed $k\rho$

$$J_0(k\rho\zeta\sqrt{\zeta^2 - i}) \sim \sqrt{\frac{2}{\pi k\rho\zeta(1-i)}}\exp(ik\rho\zeta(1-i) - i\frac{\pi}{4}). \tag{19}$$

Therefore,

$$\begin{aligned} f(\zeta) &\sim \frac{\zeta}{e^{kd\zeta^2} - e^{ikd}}\sqrt{\frac{2}{\pi k\rho\zeta(1-i)}}\exp(k\rho\zeta(1+i) - i\frac{\pi}{4}) \\ &\sim \sqrt{\frac{2\zeta}{\pi k\rho(1-i)}}\frac{e^{k\rho\zeta(1+i) - i\frac{\pi}{4}}}{e^{kd(\zeta^2 - i)}} \end{aligned}$$

and therefore for large $k$,

$$\max_{0\le\zeta\le\infty}\left|f(\zeta)\right| \sim \frac{e^{k\rho^2/4d}}{\sqrt{\pi kd}}.$$

Thus a canonical quadrature provides a stable and efficient way to evaluate (13) accurately with a computational complexity independent of the wave number provided

$$\frac{e^{k\rho^2/4d}}{\sqrt{\pi kd}} < \frac{\text{constant}}{kd} \tag{20}$$

where the integrand does not oscillate rapidly within the range $[0, C]$. In Figure 1, we display plots of $f(\zeta)$ near $\zeta = 0$ and of its logarithm in a larger region for values that satisfy (20).

On the other hand and as we anticipated, for large values of $\frac{k\rho^2}{4d}$, the integrand $f(\zeta)$ in (12) displays large and fast oscillations which cancel out to produce a significantly smaller integrated value, see Figure 2. Indeed, choosing

$$\frac{e^{k\rho^2/4d}}{\sqrt{\pi kd}} > 10^A\frac{1}{kd} \tag{21}$$

leads to difficulties in attempting to accurately determine the integral value in finite precision arithmetic since a canonical quadrature will lead to a loss

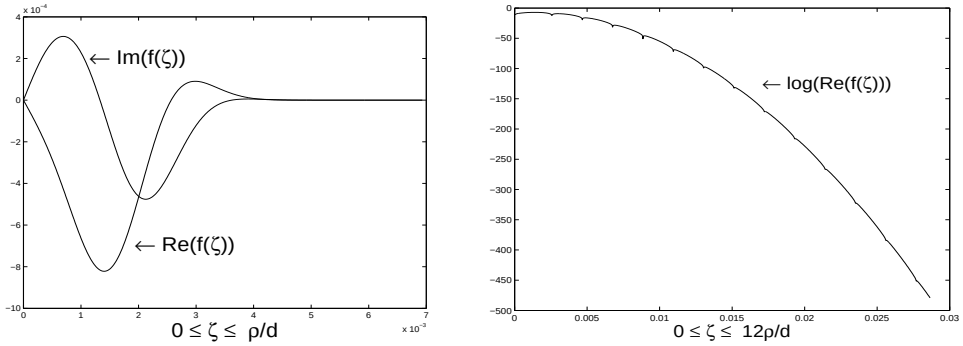


Fig. 1. The integrand $f(\zeta)$ in (14) Left: $\Re(f(\zeta))$ and $\Im(f(\zeta))$, Right: $\log(\Re(f(\zeta)))$,with $k = 10^5 + 0.2$, $d = 2\pi$, $(\rho, z) = (0.015, 0)$ and $k\rho^2/(4d) = 0.89$.

of $A$ significant digits in the value of the integral. For the sake of definiteness we shall take

$$A = 5$$

in double precision arithmetic. There remains then to design an effective way to evaluate the integral in (13) for values of $k$ and $\rho$ that falls in the regime (21).

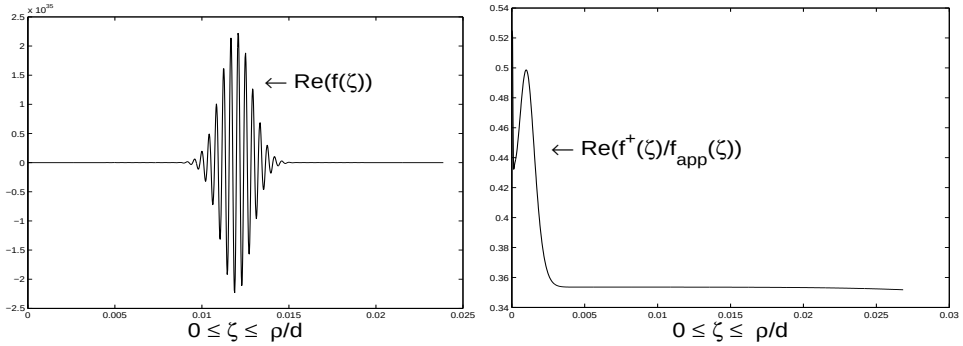


Fig. 2. The integrand $f(\zeta)$ in (14) and its approximation $\tilde{f}(\zeta)$ as defined in (19). Left: $\Re(f(\zeta))$, Right: $\Re(f(\zeta)/\tilde{f}(\zeta))$, with $k = 10^5 + 0.2$, $d = 2\pi$, $(\rho, z) = (0.15, 0)$, and $k\rho^2/(4d) = 89$.

To this end we first expand the denominator of the integrand in (14)

$$\frac{1}{e^{kd(\zeta^2-i)}-1} = \frac{1}{e^{(M+1)kd(\zeta^2-i)} - e^{Mkd(\zeta^2-i)}} + \sum_{j=1}^{M} \frac{1}{e^{jkd(\zeta^2-i)}}$$

to rewrite the integral in (17) as

$$\begin{aligned} I &= \int_0^C \zeta \frac{J_0\Big(k\rho\zeta\sqrt{\zeta^2-2i}\Big)}{e^{kd(\zeta^2-i)}-1} d\zeta \\ &= \int_0^C f_{\text{new}}^M(\zeta) d\zeta + \sum_{j=1}^{M} e^{ijkd} \int_0^C \zeta \frac{J_0\Big(k\rho\zeta\sqrt{\zeta^2-2i}\Big)}{e^{jkd\zeta^2}} d\zeta \end{aligned} \tag{22}$$

where

$$f^M_{\rm new}(\zeta) = \frac{\zeta J_0\Big(k\rho\zeta\sqrt{\zeta^2-2i}\Big)}{e^{(M+1)kd(\zeta^2-i)} - e^{Mkd(\zeta^2-i)}}. \tag{23}$$

The first integral in (22) can be treated similarly to its analogue in the case of line arrays [11–13]. Indeed we first note that choosing

$$M \approx \frac{k\rho^2}{20d}$$

allows us to capture all significant contributions to the integral. With this choice of $M$ large variations can be avoided since (see Figure 3)

$$|f^M_{\rm new}(\zeta)| \ll |f(\zeta)| \text{ and } |f^{M'}_{\rm new}(\zeta)| \ll |f^{'}(\zeta)|.$$

This in turn enables a truncation of the interval $[0, C]$ to $[0, C_{\rm new}]$ where

$$C_{\rm new} = \frac{\rho + \sqrt{\rho^2 + \frac{4Md\log(\epsilon)}{k}}}{2Md} \ll C$$

so that

$$f^M_{\rm new}(C_{\rm new}) = \epsilon$$

for any given $\epsilon$, and a canonical quadrature can be applied to evaluate the integral

$$\int_0^{C_{\rm new}} f^M_{\rm new}(\zeta)d\zeta$$

accurately with a computational complexity independent of the wave number.

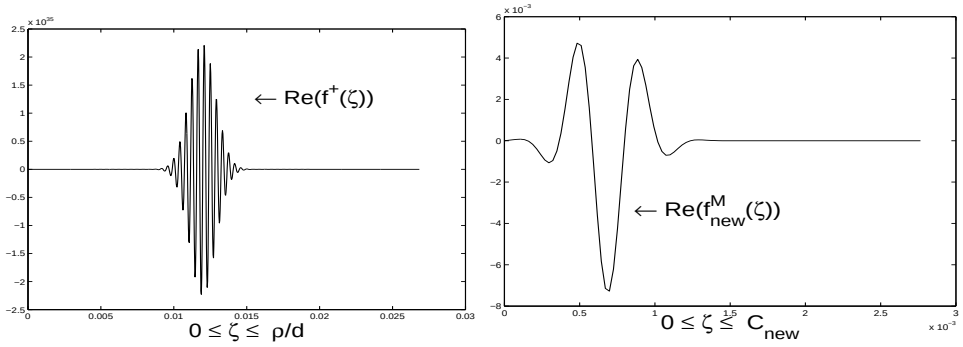


Fig. 3. The integrand $f(\zeta)$ in (12) and $f^M_{\rm new}(\zeta)$ as defined in (23). Left: $\Re(f^+(\zeta))$, Right: $\Re(f^M_{\rm new}(\zeta))$,with $k = 10^5 + 0.2$, $d = 2\pi$, $z = 0$, $\rho = 0.15$.

The treatment of the last integral in (22) however cannot proceed as in [11,12]. There the basic idea was to construct a quotient of the form

$$\frac{J_0\Big(k\rho\zeta\sqrt{\zeta^2-2i}\Big)}{J_0\Big(k\rho(1-i)\zeta\Big)} = h(\zeta) = \sum_{n=0}^{\infty} a_n\zeta^n \tag{24}$$

to allow for the representation of the integral as

$$\begin{aligned}\int_0^C \zeta \frac{J_0\Big(k\rho\zeta\sqrt{\zeta^2-2i}\Big)}{e^{jkd\zeta^2}}d\zeta &= \int_0^C \zeta \frac{J_0\Big(k\rho\zeta\sqrt{\zeta^2-2i}\Big)}{J_0\Big(k\rho(1-i)\zeta\Big)}\frac{J_0(k\rho(1-i)\zeta)}{e^{jkd\zeta^2}}d\zeta \\ &= \sum_{n=0}^{\infty} a_n \int_0^C \zeta^{n+1}\frac{J_0(k\rho(1-i)\zeta)}{e^{jkd\zeta^2}}d\zeta \\ &= \sum_{n=0}^{\infty} a_n I^{(0)}_{n+1,j}\end{aligned} \tag{25}$$

where $I^{(0)}_{n,j}$ is defined by

$$I^{(0)}_{n,j} = \int_0^C \zeta^n \frac{J_0(k\rho(1-i)\zeta)}{e^{jkd\zeta^2}}\,d\zeta. \tag{26}$$

However, in contrast when compared to the case treated in [11,12], here this procedure is numerically stable only for a much smaller region

$$k\rho^2/(2d) \leq 1$$

which does not offer any further improvement over the case where classical quadratures are effective. The difficulty arises from the size of the coefficients in (25) when $n$ is small for large $k\rho$. Indeed

$$\begin{cases} a_{2n} \sim (\dfrac{k\rho}{2})^{2n-2} \text{ for small } n \text{ and } k\rho \gg 1, \\ a_{2n+1} = 0 \text{ for } n \geq 0. \end{cases}$$

and, as shown below (cf. (38)), the integrals behave like

$$I^{(0)}_{n+1,j} \sim \frac{i\rho^{2n}}{2^{n+1}k(dj)^{2n+1}} e^{i\frac{k\rho^2}{2jd}} \text{ for } k\rho \gg 1 \text{ and } n \geq 1,$$

so that

$$a_n I^{(0)}_{n+1,j} \sim (\frac{k\rho^2}{2d})^{2n-2}.$$

As we shall show however a modification of this scheme can be used to derive a stable representation of $J_0\Big(k\rho\zeta\sqrt{\zeta^2-2i}\Big)$. More precisely, since

$$\sqrt{\zeta^2-2i} \sim 1-i \text{ for } \zeta \sim 0$$

we can expand

$$J_0\Big(k\rho\zeta\sqrt{\zeta^2-2i}\Big) = J_0\bigg((1-i)k\rho\zeta + \Big[k\rho\zeta\sqrt{\zeta^2-2i} - (1-i)k\rho\zeta\Big]\bigg)$$
$$= \sum_{n=0}^{\infty} \frac{\Big[\zeta\sqrt{\zeta^2-2i} - (1-i)\zeta\Big]^n}{n!}\bigg(D^n J_0\bigg)\Big((1-i)k\rho\zeta\Big) \quad (27)$$
$$= \sum_{n=0}^{\infty} \frac{\Big[\zeta\sum_{m=1}^{\infty} r^{2m}\zeta^{2m}\Big]^n}{n!}\bigg(D^n J_0\bigg)\Big((1-i)k\rho\zeta\Big)$$

where

$$\sqrt{\zeta^2-2i} = (1-i) + \sum_{m=1}^{\infty} r_{2m}\zeta^{2m} \text{ for } \zeta \le \sqrt{2}$$

and the coefficients $r_{2m}$ can be easily evaluated via the recursive formula

$$r_0 = 1-i \text{ and } r_{2m} = \frac{(2m-3)}{2m}\frac{(-1)^{m+1}}{2i} r_{2m-2},\ m = 1, 2, ...$$

Next, using

$$D\bigg(J_0(a)\bigg) = -J_1(a) \text{ and } D^1\bigg(J_1(a)\bigg) = J_0(a) - \frac{J_1(a)}{a},$$

the decomposition in (27) can be rewritten as

$$J_0\Big(k\rho\zeta\sqrt{\zeta^2-2i}\Big) = J_0\Big(k\rho(1-i)\zeta\Big)h_0(\zeta) + J_1\Big(k\rho(1-i)\zeta\Big)h_1(\zeta) \quad (28)$$

where

$$h_0(\zeta) = \sum_{n=0}^{\infty} b_n\zeta^n \text{ and } h_1(\zeta) = \sum_{n=0}^{\infty} c_n\zeta^n.$$

The coefficients $b_n$ and $c_n$ are explicitly given by

$$b_{2n} = \begin{cases} 1 & \text{if } n = 0, \\ 0 & \text{if } n = 1, 2, \\ \sum_{m=1}^{\lfloor \frac{n}{3} \rfloor} \dfrac{(-i)^{n+m}}{2^{n+m}} \dfrac{(n-2m-1)!(n-2m)!}{(n-3m)!(n-m)!} \dfrac{((1-i)k\rho)^{2m}}{m!(m-1)!} & \text{if } n \ge 3, \end{cases}$$

and

$$c_{2n+1} = \begin{cases} 0 & \text{if } n = 0, \\ \sum_{m=1}^{\lfloor \frac{n-1}{3} \rfloor + 1} \dfrac{(-i)^{n+m-1}}{2^{n+m}} \dfrac{n-2m+1)!(n-2m+1)!}{(n-3m+2)!(n-m+1)!} \dfrac{((1-i)k\rho)^{2m-1}}{(m-1)!^2} & \text{if } n \ge 1, \end{cases}$$

with

$$b_{2n+1} = c_{2n} = 0 \text{ for } n \ge 1$$

and where the "floor function" is defined by $\lfloor x \rfloor = \max\{n \in \mathbb{Z} \ \mid \ x \le n\}$.

This decomposition provides a more stable way to compute $J_0\Big(k\rho\zeta\sqrt{\zeta^2-2i}\Big)$ since the coefficients $b_n$ and $c_n$ are smaller than the $a_n$'s in (24)

$$b_{2n} \sim \frac{((1-i)k\rho)^{2\lfloor \frac{n}{3} \rfloor}}{(\frac{2n}{3})!2^{4n/3}} \text{ for } k\rho \gg 1 \text{ and } n \geq 3, \tag{29}$$

$$c_{2n+1} \sim \frac{((1-i)k\rho)^{2\lfloor \frac{n-1}{3} \rfloor+1}}{(\frac{2n}{3})!2^{4n/3}} \text{ for } k\rho \gg 1 \text{ and } n \geq 1. \tag{30}$$

Then, substituting (28) into (22) we obtain

$$\begin{aligned}\int_0^C \zeta \frac{J_0\Big(k\rho\zeta\sqrt{\zeta^2-2i}\Big)}{e^{jkd\zeta^2}} d\zeta &= \sum_{n=0}^{\infty} b_n \bigg[ \int_0^C \zeta^{n+1} \frac{J_0(k\rho(1-i)\zeta)}{e^{jkd\zeta^2}}\, d\zeta \bigg] \\ &\qquad + \sum_{n=0}^{\infty} c_n \bigg[ \int_0^C \zeta^{n+1} \frac{J_1(k\rho(1-i)\zeta)}{e^{jkd\zeta^2}}\, d\zeta \bigg] \\ &= \sum_{n=0}^{\infty} b_n I^{(0)}_{n+1,j} + \sum_{n=0}^{\infty} c_n I^{(1)}_{n+1,j} \\ &= \sum_{n=0}^{\infty} b_{2n} I^{(0)}_{2n+1,j} + \sum_{n=1}^{\infty} c_{2n+1} I^{(1)}_{2n+2,j}.\end{aligned} \tag{31}$$

where

$$I^{(1)}_{n,j} = \int_0^C \zeta^n \frac{J_1\Big(k\rho(1-i)\zeta\Big)}{e^{jkd\zeta^2}}\, d\zeta.$$

and $I^{(0)}_{n,j}$ is as in (26).

The evaluation of the integrals $I^{(0)}_{2n+1,j}$ and $I^{(1)}_{2n,j}$ in (31) is clearly preferable to that in (13), on account of the diminishing values and faster decay of the former as $j$ increases. Moreover, as we show next, $I^{(0)}_{2n+1,j}$ and $I^{(1)}_{2n,j}$ can be computed explicitly, with the use of Hankel's formula [14]:

$$\int_0^{\infty} \zeta^{\mu-1} \frac{J_\nu\Big(a\zeta\Big)}{e^{p^2\zeta^2}}\, d\zeta = \frac{\Gamma(\frac{1}{2}\nu + \frac{1}{2}\mu)(\frac{1}{2}a/p)^\nu}{2p^\mu \Gamma(\nu+1)} {}_1F_1(\frac{1}{2}\nu+\frac{1}{2}\mu; \nu+1; -\frac{a^2}{4p^2}), \text{ if } \Re(\mu+\nu) > 0, \tag{32}$$

where ${}_1F_1$ denotes the confluent hypergeometric function of the first kind.

To this end we will first consider the evaluation of $I^{(0)}_{2n+1,j}$ and let

$$V^{(0)}_{2n+1,j} = \int_0^{\infty} \zeta^{2n+1} \frac{J_0\Big(k\rho(1-i)\zeta\Big)}{e^{kdu^2}} d\zeta$$

Then from (32) (with $\nu = 0$ and $\mu = 2n + 2$)

$$V^{(0)}_{2n+1,j} = \frac{n!}{2(kdj)^{n+1}} {}_1F_1(n+1, 1; \frac{ik\rho^2}{2dj}) \tag{33}$$

where for fixed $b$ the hypergeometric function ${}_1F_1(n, b; \frac{ik\rho^2}{2dj})$ can be evaluated through the recursive formula [9, Equation 13.4.1]

$${}_1F_1(a+1, b, c) = \frac{(c+2a-b)}{a} {}_1F_1(a, b, c) + \frac{(b-a)}{a} {}_1F_1(a-1, b, c), \tag{34}$$

with

$${}_1F_1(b, b; c) = e^c \text{ and } {}_1F_1(b+1, b; c) = \frac{(c+b)}{b}, \tag{35}$$

with $b = 1$. Alternatively ${}_1F_1(n, 1; \frac{ik\rho^2}{2dj})$ can be evaluated explicitly as

$${}_1F_1(n+b, b; \frac{ik\rho^2}{2dj}) = e^{i\frac{k\rho^2}{2dj}} \sum_{m=0}^{n} \frac{n!}{m!(n-m)!(n-m+b-1)!} (i\frac{k\rho^2}{2dj})^{n-m}.$$

As we shall see $V^{(0)}_{2n+1,j}$ provides a good approximation to $I^{(0)}_{2n+1,j}$ for $n$ small. For $n$ large, on the other hand, it follows from (33) that

$$V^{(0)}_{2n+1,j} \to \infty \text{ as } n \to \infty$$

and these values do not provide a good estimate of $I^{(0)}_{2n+1,j}$. However, in this case, we can simply estimate

$$|I^{(0)}_{n,j}| < \epsilon C^{n+1} \text{ for } n > N,$$

where $\epsilon$ is as in (16), provided

$$N = \frac{k\rho^2}{8d} - \frac{\log(\epsilon)}{2} + \frac{k\rho}{4d}\sqrt{\rho^2 - \frac{4d\log(\epsilon)}{k}}.$$

Given such $N$ then we have

$$|I^{(0)}_{n,j} - V^{(0)}_{n,j}| \leq \epsilon C^n \text{ for } n \leq N.$$

A similar argument delivers

$$|I^{(1)}_{n,j}| < \epsilon C^{n+1} \text{ for } n > N,$$

and

$$|I^{(1)}_{n,j} - V^{(1)}_{n,j}| \leq \epsilon C^n \text{ for } n \leq N,$$

where

$$V_{2n,j}^{(1)} = \int_0^\infty \zeta^{2n} \frac{J_1\Big(k\rho(1-i)\zeta\Big)}{e^{kdu^2}} d\zeta.$$

As before, from (32) ($\nu = 1$ and $\mu = 2n+3$), we have

$$V_{2n,j}^{(1)} = \frac{\Gamma(n+2)(k\rho(1-i))}{4(kdj)^{n+2}} {}_1F_1(n+2, 2; \frac{ik\rho^2}{2dj}) \tag{36}$$

where ${}_1F_1(n, 2; \frac{ik\rho^2}{2dj})$ can again be calculated through (34) and (35) (with $b = 2$).

Finally using (33) and (36) the Green's function $G(\rho, 0)$ can be written as

$$\begin{aligned} G(\rho,0) \approx \frac{e^{ik\rho}}{4\pi\rho} &+ \frac{k}{\pi}\int_0^{C_{\text{new}}} f_{\text{new}}^M(\zeta)\, d\zeta \\ &+ \frac{k}{\pi}\sum_{j=1}^{M} e^{ikjd} \sum_{n=0}^{N} b_{2n} \frac{n!}{2(kdj)^{n+1}} {}_1F_1(n+1, 1; \frac{ik\rho^2}{2dj}) \\ &+ \frac{k}{\pi}\sum_{j=1}^{M} e^{ikjd} \sum_{n=1}^{N} c_{2n+1} \frac{(n+1)!(k\rho(1-i))}{4(kdj)^{n+2}} {}_1F_1(n+2, 2; \frac{ik\rho^2}{2dj}). \end{aligned} \tag{37}$$

To see that (37) improves on the stability of a direct application of (13) we first note that

$$\frac{n!}{2(kdj)^{n+1}} {}_1F_1(n+1, 1; \frac{ik\rho^2}{2dj}) \sim \frac{i\rho^{2n} e^{i\frac{k\rho^2}{2jd}}}{2^{n+1}k(dj)^{2n+1}} \text{ for } k\rho \gg 1 \text{ and } n \geq 1, \tag{38}$$

and using (29), the terms in the first inner sum decay as

$$\left| b_{2n} \frac{n!}{2(kdj)^{n+1}} {}_1F_1(n+1, 1; \frac{ik\rho^2}{2dj}) \right| \sim \frac{1}{2kdj} \left( \frac{k\rho^4}{8\sqrt{2}(dj)^3} \right)^{2n/3} \frac{1}{(2n/3)!} \text{ for } n \geq 1. \tag{39}$$

A similar argument applies to the second inner sum in (37). In this case

$$\frac{(n+1)!(k\rho(1-i))}{4(kdj)^{n+2}} {}_1F_1(n+2, 2; \frac{ik\rho^2}{2dj}) \sim \frac{(1+i)\rho^{2n-1} e^{i\frac{k\rho^2}{2jd}}}{2^{n+1}k(dj)^{2n}} \text{ for } k\rho \gg 1 \text{ and } n \geq 1,$$

and, using (30), we see that

$$\left| c_{2n+1} \frac{(n+1)!(k\rho(1-i))}{4(kdj)^{n+2}} {}_1F_1(n+2, 2; \frac{ik\rho^2}{2dj}) \right| \sim \frac{1}{2(k\rho)^{2/3}} \left( \frac{k\rho^4}{16d^3j^3} \right)^{2n/3} \text{ for } n \geq 1. \tag{40}$$

Finally we note that, for stability, (39) and (40) demand only that

$$\frac{k\rho^4}{d^3} < \text{ constant}$$

which significantly improves upon (13); see Tables 5– 8.

## 5 Set of Numerical Results

In this section, we provide two sets of numerical experiments where we compare the values and computational times associated with the Green's function $G(\rho, z) = G(x, y, z)$ obtained from the new integral representation (11), the classical spatial and spectral representations(cf. (1), (3)), and the Ewald's transform (4). More precisely these sets correspond to the cases when $k\rho^2/(4d) \lesssim 1$ and $1 \ll k\rho^2/(4d)$, respectively.

The implementation of every scheme is largely straightforward, as it entails evaluations of standard special functions and simple sums and products. For the Ewald method the necessary evaluations of the complementary error function – for complex arguments – are performed using the algorithm in [15]. The method introduced above, on the other hand, relies on the evaluation of integrals (cf. $I^M_{\text{new}}$ in (23)) with integrands that display exponentially small (odd order) derivatives at the boundary of the integration domain and are thus amenable to very accurate evaluations via the trapezoidal rule.

For comparison purposes, and to ensure the accuracy of both representations, all calculations were performed in double precision arithmetic. For the evaluation of the relative error

$$\text{Err} = \frac{|G^{\text{Exact}}(\rho, z) - G^{\text{Method}}(\rho, z)|}{|G^{\text{Exact}}(\rho, z)|} \tag{41}$$

an "exact solution" $G^{\text{Exact}}(\rho, z)$ was computed in quadruple precision arithmetic (using the spectral representation to avoid biases). The tables confirm the expected behavior of each methodology, as discussed above.

In both tests the sums in the spatial representation are truncated for $\text{N}_1 = 10^5$ and $\text{N}_2 = 10^6$ to display the first order convergence demonstrated in (2). Truncation for the spectral representation, on the other hand, is based on the exponential convergence of the method. The Ewald transformation, on the other hand, displays a stronger instability, enhanced for increasing $\rho$, as the values of the wave number exceed the ratio $\max\{\sqrt{\rho^2 + z^2}/\rho^2, 1/\rho\}$ (cf. (10)). The cases where this method does not converge ("dnc") are labeled as such.

In the first set of the numerical experiments (Tables 1-4), we consider the case where $d = 2\pi$, $z = 0.1$ for $\rho = 0.001$ and $\rho = \sqrt{d/k}$ leading to values $k\rho^2/(4d) \lesssim 1$. Here $\alpha = 0$, for (Tables 1-2) and $\alpha = k\sin(\frac{\pi}{3})$, for (Tables 3-4) In the second set, (Tables 5-8), on the other hand, we let $d = 2\pi$, $\alpha = 0$, $z = 0$ for $\rho = 0.01, 0.1, 0.3$ and $\rho = 0.5$ which lead to values $1 \ll k\rho^2/(4d)$.

As the tables show, the schemes introduced here can be seen to consistently outperform the alternative procedures within its domain of applicability, where it delivers higher accuracy in shorter computational times.

Table 1
Error (41) and computational times ($t$) for evaluation of $G(\rho, z)$ with $\alpha = 0,\ k = 10^n + 0.2,\ (\rho, z) = (0.001, 0.1)$.

| $n$ | Spa. | $t_{Spa.}^{N_1}$ | Spa. | $t_{Spa.}^{N_2}$ | Spe. | $t_{Spe.}$ | Ewa. | $t_{Ewa.}$ | NA | $t_{NA}$ |
|---|---|---|---|---|---|---|---|---|---|---|
| 1 | 1.4e-7 | 0.3s | 1.4e-8 | 3s | 3e-15 | 5s | 1.9e-16 | 0.1s | 3e-16 | 0.2s |
| 2 | 2.2e-7 | 0.3s | 2.2e-8 | 3s | 6e-15 | 5s | 5.8e-14 | 0.2s | 2e-15 | 0.2s |
| 3 | 2.4e-7 | 0.3s | 2.4e-8 | 3s | 9e-15 | 5s | 1.1e-13 | 2s | 7e-15 | 0.2s |
| 4 | 1.4e-7 | 0.3s | 1.4e-8 | 3s | 2e-13 | 5s | 4.8e-13 | 40s | 2e-13 | 0.2s |
| 5 | 2.5e-7 | 0.3s | 2.5e-8 | 3s | 7e-13 | 17s | dnc | ... | 6e-12 | 0.2s |
| 6 | 2.7e-7 | 0.3s | 2.7e-8 | 3s | 9e-12 | 163s | dnc | ... | 3e-11 | 0.2s |
| 7 | 2.6e-7 | 0.3s | 2.6e-8 | 3s | 1e-10 | 1648s | dnc | ... | 2e-10 | 0.2s |

Table 2
Error (41) and computational times ($t$) for evaluation of $G(\rho, z)$ with $\alpha = 0,\ k = 10^n + 0.2,\ (\rho, z) = (\sqrt{d/k}, 0.1)$.

| $n$ | Spa. | $t_{Spa.}^{N_1}$ | Spa. | $t_{Spa.}^{N_2}$ | Spe. | $t_{Spe.}$ | Ewa. | $t_{Ewa.}$ | NA | $t_{NA}$ |
|---|---|---|---|---|---|---|---|---|---|---|
| 1 | 9.9e-7 | 0.3s | 9.9e-8 | 3s | 1e-15 | 0.1s | 1.1e-13 | 0.1s | 2e-15 | 0.2s |
| 2 | 6.6e-7 | 0.3s | 6.6e-8 | 3s | 3e-15 | 0.1s | dnc | ... | 1e-15 | 0.2s |
| 3 | 2.9e-7 | 0.3s | 2.9e-8 | 3s | 1e-14 | 0.2s | dnc | ... | 8e-15 | 0.2s |
| 4 | 1.5e-7 | 0.3s | 1.5e-8 | 3s | 1e-13 | 1.6s | dnc | ... | 2e-13 | 0.2s |
| 5 | 2.5e-7 | 0.3s | 2.5e-8 | 3s | 1e-12 | 16s | dnc | ... | 6e-12 | 0.2s |
| 6 | 2.7e-7 | 0.3s | 2.7e-8 | 3s | 1e-11 | 163s | dnc | ... | 2e-11 | 0.2s |
| 7 | 2.6e-7 | 0.3s | 2.6e-8 | 3s | 1e-10 | 1645s | dnc | ... | 2e-10 | 0.2s |

Table 3
Error (41) and computational times ($t$) for evaluation of $G(\rho, z)$ with $\alpha = k\sin(\frac{\pi}{3})$, $k = 10^n + 0.2$, $(\rho, z) = (0.001, 0.1)$.

| $n$ | Spa. | $t_{Spa.}^{N_1}$ | Spa. | $t_{Spa.}^{N_2}$ | Spe. | $t_{Spe.}$ | Ewa. | $t_{Ewa.}$ | NA | $t_{NA}$ |
|---|---|---|---|---|---|---|---|---|---|---|
| 1 | 7.1e-07 | 0.5s | 7.6e-08 | 5s | 1.0e-14 | 7s | 2.1e-14 | 0.1s | 1.8e-15 | 0.2s |
| 2 | 1.1e-06 | 0.5s | 1.1e-07 | 5s | 2.0e-14 | 7s | 2.9e-12 | 0.4s | 6.7e-16 | 0.2s |
| 3 | 1.7e-05 | 0.5s | 1.7e-06 | 5s | 5.5e-13 | 7s | 5.6e-13 | 4s | 6.3e-13 | 0.2s |
| 4 | 1.7e-07 | 0.5s | 4.3e-09 | 5s | 1.2e-13 | 7s | 9.3e-13 | 110s | 1.8e-13 | 0.2s |
| 5 | 3.4e-07 | 0.5s | 3.5e-08 | 5s | 2.6e-12 | 30s | dnc | ... | 2.6e-12 | 0.2s |
| 6 | 2.0e-07 | 0.5s | 2.2e-08 | 5s | 1.6e-11 | 275s | dnc | ... | 1.2e-11 | 0.2s |
| 7 | 2.1e-06 | 0.5s | 2.5e-07 | 5s | 5.6e-10 | 2900s | dnc | ... | 2.8e-10 | 0.2s |

Table 4
Error (41) and computational times ($t$) for evaluation of $G(\rho, z)$ with $\alpha = k\sin(\frac{\pi}{3})$, $k = 10^n + 0.2$, $(\rho, z) = (\sqrt{d/k}, 0.1)$.

| $n$ | Spa. | $t_{Spa.}^{N_1}$ | Spa. | $t_{Spa.}^{N_2}$ | Spe. | $t_{Spe.}$ | Ewa. | $t_{Ewa.}$ | NA | $t_{NA}$ |
|---|---|---|---|---|---|---|---|---|---|---|
| 1 | 6.2e-06 | 0.5s | 6.6e-07 | 5s | 1.1e-14 | 0.1s | 1.4e-13 | 0.2s | 1.8e-14 | 0.2s |
| 2 | 2.6e-06 | 0.5s | 2.7e-07 | 5s | 3.1e-15 | 0.1s | dnc | ... | 5.7e-15 | 0.2s |
| 3 | 2.4e-05 | 0.5s | 2.4e-06 | 5s | 8.2e-13 | 0.3s | dnc | ... | 9.2e-13 | 0.2s |
| 4 | 1.7e-07 | 0.5s | 4.4e-09 | 5s | 1.5e-13 | 3s | dnc | ... | 2.6e-13 | 0.2s |
| 5 | 3.3e-07 | 0.5 s | 3.4e-08 | 5s | 1.1e-12 | 27s | dnc | ... | 7.1e-12 | 0.2s |
| 6 | 2.0e-07 | 0.5 s | 2.0e-08 | 5s | 1.9e-11 | 278s | dnc | ... | 2.1e-11 | 0.2s |
| 7 | 2.2e-06 | 0.5 s | 2.3e-07 | 5s | 5.7e-10 | 2850s | dnc | ... | 2.6e-10 | 0.2s |

## Appendix A: Formulation of the new algorithm for arbitrary incidence and evaluation points

In this appendix we provide the details on the extension of the formulas (13)–(17) to the most general case. For this we look at the integral representation given by (11)–(12)

$$G(\rho, z) = \frac{1}{4\pi}\frac{e^{ikr_0}}{r_0} + \frac{k}{2\pi}\Big[\int_0^\infty f^{(1)}(\zeta)d\zeta + \int_0^\infty f^{(2)}(\zeta)d\zeta\Big]$$

Table 5
Error (41) and computational times ($t$) for evaluation of $G(\rho, z)$ with $\alpha = 0, k = 10^n + 0.2, (\rho, z) = (0.01, 0)$.

| $n$ | Spa. | $t_{\text{Spa.}}^{N_1}$ | Spa. | $t_{\text{Spa.}}^{N_2}$ | Spe. | $t_{\text{Spe.}}$ | Ewa. | $t_{\text{Ewa.}}$ | NA | $t_{\text{NA}}$ |
|---|---|---|---|---|---|---|---|---|---|---|
| 1 | 2.7e-08 | 0.3s | 2.7e-09 | 3s | 4.1e-15 | 0.5s | 1.1e-15 | 0.1s | 1.1e-16 | 0.2s |
| 2 | 2.7e-08 | 0.3s | 2.7e-09 | 3s | 1.2e-15 | 0.5s | 2.8e-12 | 0.2s | 1.1e-16 | 0.2s |
| 3 | 2.7e-08 | 0.3s | 2.7e-09 | 3s | 4.8e-15 | 0.5s | 1.3e-10 | 2s | 9.0e-16 | 0.2s |
| 4 | 2.7e-08 | 0.3s | 2.7e-09 | 3s | 1.2e-14 | 1s | dnc | ... | 9.8e-15 | 0.2s |
| 5 | 2.7e-08 | 0.3s | 2.6e-09 | 3s | 1.0e-13 | 9s | dnc | ... | 8.4e-14 | 0.2s |
| 6 | 2.7e-08 | 0.3s | 2.5e-09 | 3s | 1.5e-12 | 89s | dnc | ... | 5.6e-12 | 0.2s |
| 7 | 2.7e-08 | 0.3s | 2.5e-09 | 3s | 1.5e-12 | 890s | dnc | ... | 5.6e-12 | 0.2s |

Table 6
Error (41) and computational times ($t$) for evaluation of $G(\rho, z)$ with $\alpha = 0, k = 10^n + 0.2, (\rho, z) = (0.1, 0)$.

| $n$ | Spa. | $t_{\text{Spa.}}^{N_1}$ | Spa. | $t_{\text{Spa.}}^{N_2}$ | Spe. | $t_{\text{Spe.}}$ | Ewa. | $t_{\text{Ewa.}}$ | NA | $t_{\text{NA}}$ |
|---|---|---|---|---|---|---|---|---|---|---|
| 1 | 2.6e-07 | 0.3s | 3s | 2.6e-08 | 8.9e-16 | 0.5s | 2.0e-14 | 0.1s | 4.3e-16 | 0.2s |
| 2 | 2.7e-07 | 0.3s | 3s | 2.7e-08 | 1.4e-15 | 0.5s | 1.7e-12 | 0.1s | 1.6e-15 | 0.2s |
| 3 | 2.8e-07 | 0.3s | 3s | 2.8e-08 | 4.2e-15 | 0.5s | dnc | ... | 3.4e-15 | 0.2s |
| 4 | 2.6e-07 | 0.3s | 3s | 2.6e-08 | 5.7e-13 | 1s | dnc | ... | 8.7e-14 | 0.2s |
| 5 | 2.7e-07 | 0.3s | 3s | 2.7e-08 | 1.4e-12 | 9s | dnc | ... | 7.1e-13 | 0.2s |
| 6 | 2.7e-07 | 0.3s | 3s | 2.4e-08 | 3.9e-11 | 85s | dnc | ... | 1.5e-10 | 0.4s |

Table 7
Error (41) and computational times ($t$) for evaluation of $G(\rho, z)$ with $\alpha = 0, k = 10^n + 0.2, (\rho, z) = (0.3, 0)$.

| $n$ | Spa. | $t_{\text{Spa.}}^{N_1}$ | Spa. | $t_{\text{Spa.}}^{N_2}$ | Spe. | $t_{\text{Spe.}}$ | Ewa. | $t_{\text{Ewa.}}$ | NA | $t_{\text{NA}}$ |
|---|---|---|---|---|---|---|---|---|---|---|
| 1 | 7.8e-07 | 0.3s | 7.8e-08 | 3s | 2.2e-16 | 0.1s | 4.5e-14 | 0.1s | 1.1e-15 | 0.2s |
| 2 | 8.8e-07 | 0.3s | 8.8e-08 | 3s | 4.8e-15 | 0.1s | dnc | ... | 4.7e-15 | 0.2s |
| 3 | 8.9e-07 | 0.3s | 8.9e-08 | 3s | 2.8e-14 | 0.1s | dnc | ... | 5.0e-14 | 0.2s |
| 4 | 7.7e-07 | 0.3s | 7.7e-08 | 3s | 2.4e-12 | 1s | dnc | ... | 3.9e-13 | 0.2s |
| 5 | 8.3e-07 | 0.3s | 8.1e-08 | 3s | 3.1e-11 | 10s | dnc | ... | 3.5e-11 | 0.6s |
| 6 | 7.5e-07 | 0.3s | 8.2e-08 | 3s | 4.6e-10 | 100s | dnc | ... | 1.0e-02 | 2s |

where

$$f^{(1)}(\zeta) = e^{ikz}\zeta \frac{e^{i(k-\alpha)d}e^{-kz\zeta^2}}{e^{kd\zeta^2} - e^{i(k-\alpha)d}} J_0\Big(k\rho\zeta\sqrt{\zeta^2 - 2i}\Big)d\zeta,$$

$$f^{(2)}(\zeta) = e^{-ikz}\zeta \frac{e^{i(k+\alpha)d}e^{kz\zeta^2}}{e^{kd\zeta^2} - e^{i(k+\alpha)d}} J_0\Big(k\rho\zeta\sqrt{\zeta^2 - 2i}\Big)d\zeta,$$

Table 8
Error (41) and computational times ($t$) for evaluation of $G(\rho, z)$ with $\alpha = 0, k = 10^n + 0.2, (\rho, z) = (0.5, 0)$.

| $n$ | Spa. | $t^{N_1}_{Spa.}$ | Spa. | $t^{N_2}_{Spa.}$ | Spe. | $t_{Spe.}$ | Ewa. | $t_{Ewa.}$ | NA | $t_{NA}$ |
|---|---|---|---|---|---|---|---|---|---|---|
| 1 | 1.6e-06 | 0.3s | 1.6e-07 | 3s | 2.1e-16 | 0.1s | 3.4e-14 | 0.1s | 1.2e-15 | 0.2s |
| 2 | 1.6e-06 | 0.3s | 1.6e-07 | 3s | 7.7e-15 | 0.1s | dnc | ... | 1.6e-14 | 0.2s |
| 3 | 1.2e-06 | 0.3s | 1.2e-07 | 3s | 3.5e-14 | 0.1s | dnc | ... | 9.4e-14 | 0.2s |
| 4 | 1.3e-06 | 0.3s | 1.3e-07 | 3s | 6.1e-12 | 1s | dnc | ... | 2.5e-12 | 0.2s |
| 5 | 1.5e-06 | 0.3s | 1.4e-07 | 3s | 8.4e-11 | 9s | dnc | ... | 1.3e-03 | 0.6s |
| 6 | 1.2e-06 | 0.3s | 1.2e-07 | 3s | 8.5e-10 | 95s | dnc | ... | 3.7e+07 | 7s |

note that for $\alpha = 0$ and $z = 0$, we have $f^{(1)}(\zeta) = f^{(2)}(\zeta)$. As in (4.1) these integrals are truncated to the intervals

$$C^{1,2} = \frac{\rho + \sqrt{\rho^2 - \frac{4(d \pm z)\log(\epsilon)}{k}}}{2(d \pm z)}$$

Finally Green's function can be approximated by

$$G(\rho, z) \approx \frac{1}{4\pi}\frac{e^{ikr_0}}{r_0} + \frac{k}{2\pi}\Big[\int_0^{C^1} f^{(1)}(\zeta)d\zeta + \int_0^{C^2} f^{(2)}(\zeta)d\zeta\Big].$$

## References


[1] H.F. Olson, *Acoustical Engineering*, Princeton, N.J., Van Nostrand, 1957.

[2] Twersky V., *On the scattering of waves by an infinite grating*, IRE Trans. on Antennas Propagation 4, 1956, 330-345.

[3] Linton C. M., *The Green's Function for the two-dimensional Helmholtz Equation in Periodic Domain*, Journal of Engineering Mathematics 33, 1998, 377-402.

[4] Pozrikidis, C. *Computation of periodic Green's functions of Stokes flow,* Journal of Engineering Mathematics, 30 1996, pp. 79-96.

[5] K. E. Jordan, G. R. Richter, P. Sheng, *An efficient numerical evaluation of the Greens function for the Helmholtz operator on periodic structures,* Journal of Computational Physics 63, 1986, pp. 222-235.

[6] Jorgenson, R. E. and R. Mittra, *Efficient Calculation of the Free Space Periodic Greens Function,* IEEE Trans. Antennas Propagat., 38, 633-642, 1990.

[7] F. Capolino, D.R. Wilton, W.A. Johnson *Efficient computation of the 3D Green's function for the Helmholtz operator for a linear array of point sources*

*using the Ewald method*, Journal of Computational Physics, 223, 2007, pp. 250-261.

[8] Mathis A. W., Peterson A. F., *A comparison of acceleration procedures for the two-dimensional periodic Green's function*, in IEEE Trans. Antennas Propagat., 44, 1996, pp. 567-571.

[9] Abramowitz M. and Stegun I. A., eds. (1972), *Handbook of Mathematical Functions with Formulas, Graphs, and Mathematical Tables,* New York: Dover Publications 1964.

[10] A. Erdèlyi, W. Magnus, F. Oberhettinger, and F. G. Tricomi, *Tables of Integral Transforms*, vol. 1 New York: McGraw-Hill, 1954.

[11] Kurkcu H. and Reitich F., *Efficient calculation of the Green's functions for the two-dimensional Helmholtz equation in periodic domains*, in Proceedings of the 8th International Conference on Mathematical and Numerical Aspects of Waves, 2007.

[12] Kurkcu H. and Reitich F., *Stable and efficient evaluation of periodized Green's functions for the Helmholtz equation at high frequencies*, in Journal of Computational Physics, 228, 2009 pp. 75-95.

[13] Kurkcu H. and Reitich F., *Precise evaluation of the periodized Green's function for the Helmholtz equation at high frequencies*, in Proceedings of the Advanced Computational Methods in Engineering, 2008.

[14] Watson G. N., *A Treatise on the Theory of Bessel Functions*, Cambridge University Press, 1922.

[15] Zhang S., Jin J., *Computation of Special Functions*, Wiley, (1996).